Journal of Volcanology and Geothermal Research 421 (2022) 107451

Contents lists available at ScienceDirect

Journal of Volcanology and Geothermal Research

journal homepage: www.elsevier.com/locate/jvolgeores

Recent seismicity at Ceboruco Volcano (Mexico)

Diana Núñez [a,*], Francisco J. Núñez-Cornú [a], Charlotte A. Rowe [b]

[a] CA276 Sismología y Volcanología de Occidente (SisVOc), Universidad de Guadalajara, Puerto Vallarta, Jalisco, Mexico
[b] Los Alamos National Laboratory, NM, USA

ARTICLE INFO

Article history:
Received 1 September 2021
Received in revised form 1 December 2021
Accepted 6 December 2021
Available online 10 December 2021

Keywords:
Ceboruco Volcano
Volcano seismology
Seismic swarms
Seismic families
Volcano-tectonics
Seismic sequences

ABSTRACT

Magma and related hydrothermal fluid movement, and their interaction with solid rock, in active volcanic regions, generate a wide variety of seismic waves whose characterization can mitigate the risk of a potential eruption. Located in the western region of the Trans-Mexican Volcanic Belt, Ceboruco Volcano, whose last eruptive period was 1870–1875, is considered to be one of the most hazardous volcanoes in Mexico. We have conducted a detailed study of the seismicity in the surroundings of Ceboruco's volcanic edifice to assess the current state of this volcano. A dense temporary seismic network with 25 seismic stations in an area of 16 km × 16 km was deployed between November 2016 and July 2017, as part of the P-24 project of the CeMIEGeo consortium; this effort has allowed the detection of 81 earthquakes concentrated beneath the crater with depths between 4 and 8 km. In this study, We observe that the recorded seismicity occurs in swarms, and we specifically identify four sequences that we characterize in detail via the first focal mechanisms available for this volcano. Our results suggest a change in the local seismicity distribution compared to earlier observations, which reported seismic activity near the volcano edifice associated with fluid migration along zones of weakness related to the extensional stresses of the Tepic-Zacoalco rift. The changes in seismic patterns and obtained focal mechanisms are consistent with observed fluid effects at many geothermal sites worldwide, but also could suggest resumption of activity at this currently dormant volcano.

1. Introduction

Ceboruco Volcano is an active stratovolcano located in northwestern Mexico (Fig. 1*a*). The volcano has a truncated conical shape and asymmetric relief with a maximum height of 2280 m at its highest point, La Coronilla, in the inner crater (Fig. 1*b*). The volcano's edifice exhibits a difference in elevation of 1160 m on its eastern and southeastern flanks related to the remnants of the ancient volcanic edifice and 850 m on its northwestern flanks characterized by more recent lavas.

The onset of its volcanism is unknown since the oldest lavas are not exposed at the surface, and pyroclastic deposits are absent in the surrounding valleys. Therefore, it is assumed that there were no violent explosive eruptions during the early construction of the volcanic edifice. This period is termed the pre-Jala stage. The oldest known age is 370 ± 2 ka (Ferrari et al., 1997), at which time the volcano may have reached an altitude of 2700 m with a conical shape, and extruded a volume of 45–60 km^3 of lavas of andesitic composition (Nelson, 1980; Nelson, 1986; Sieron, 2009) (Fig. 1*c*).

The Plinian Jala Eruption was responsible for the formation of the outer crater of the volcano. Subsequently, the Dos Equis dome was emplaced and laterally drained towards the south by the dacitic Copales lava flow. Deflation and subsidence associated with this event produced the inner crater. Lava flows of andesitic and andesitic-basaltic composition within a period of 150 years after the Jala Eruption formed the current appearance of the volcano (Böhnel et al., 2016). The absence of deposits on its slopes and other information indicates that there may have been a period of inactivity of 700 years.

In February 1870, Ceboruco Volcano resumed its activity, producing ashfall, basalt blocks and pyroclastic flows. Later, a dacitic lava flow (VEI 3) was extruded and, within two years, reached 8 km in length in the direction of the town of Uzeta, SW of the volcano (Fig. 1b). Contemporary historical reports (e.g., Caravantes, 1870; Banda, 1871; Iglesias, 1875; Iglesias et al., 1877; Barrera, 1931) compiled observations on underground noise, seismic activity, and white steam above the volcano in 1783 and 1832 and closer in time to the eruption. Some of these authors reported constant seismic activity prior to the eruption, prompting inhabitants of Jala to leave their houses for a few days. As many as eight vents were observed, through which steam, ash, and incandescent material were released. The eruptive activity of the volcano ceased in 1875. Since then, fumarolic activity has been observed in the inner and outer

* Corresponding author at: Av. Universidad, 203. Del. Ixtapa, Puerto Vallarta, Jalisco Zip Code 48280, Mexico
E-mail address: diana@sisvoc.mx (D. Núñez).

https://doi.org/10.1016/j.jvolgeores.2021.107451

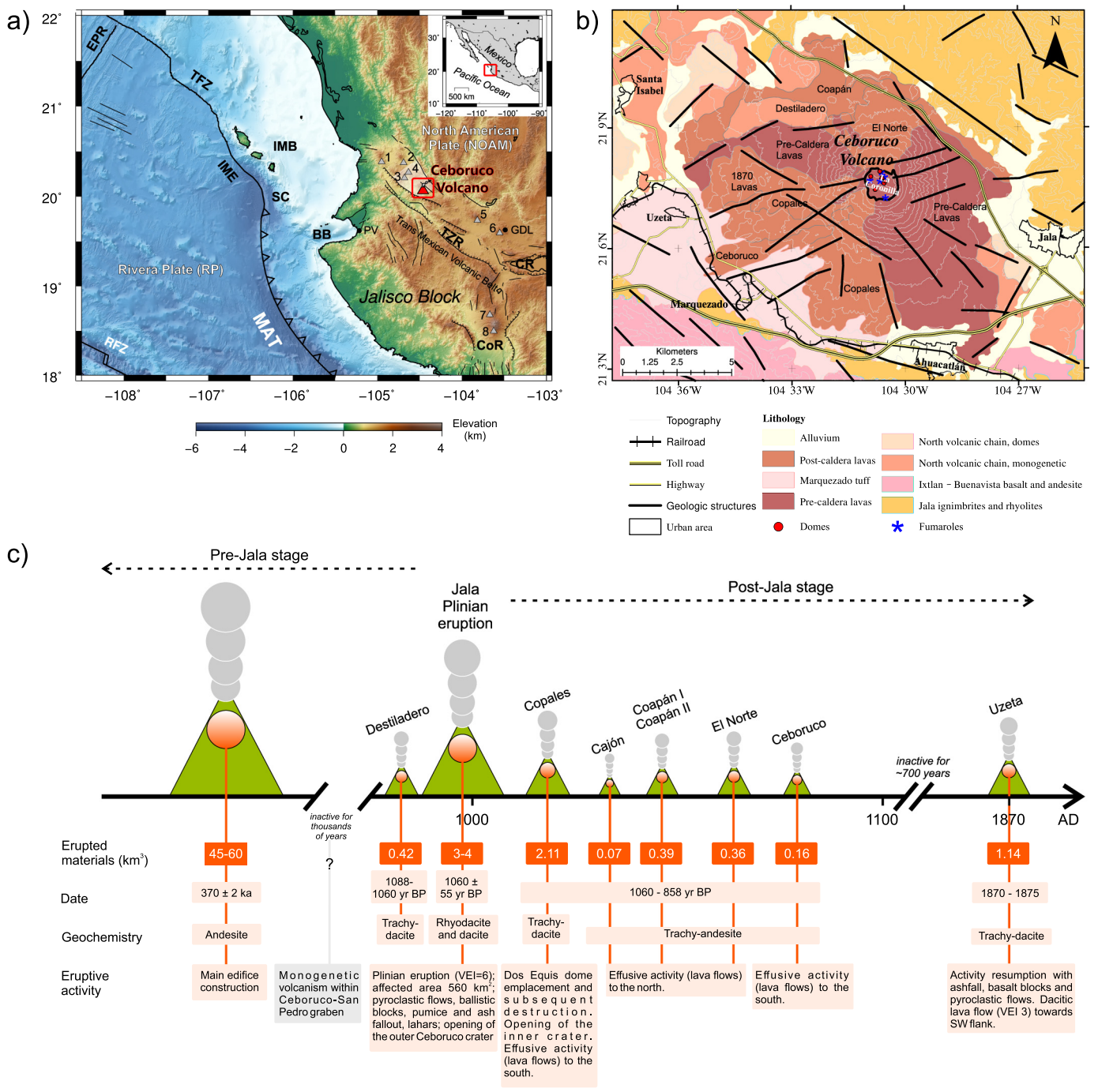

Fig. 1. a) Western Mexico tectonic framework. *Abbreviations*: *BB*, Bahía de Banderas; *CoR*, Colima rift; *CR*, Chapala rift; *EPR*, East Pacific rise; *GDL*, Guadalajara; *IMB*, Islas Marías block; *IME*, Islas Marías escarpment; *MAT*, Middle America trench; *PV*, Puerto Vallarta; *RFZ*, Rivera fracture zone; *SC*, Sierra de Cleofas; *TFZ*, Tamayo fault zone; *TZR*, Tepic–Zacoalco rift; *1*, San Juan; *2*, Sangangüey; *3*, San Pedro Complex; *4*, Tepetiltic Volcano; *5*, Tequila Volcano; *6*, La Primavera Caldera; *7*, Colima; *8*, Nevado de Colima. Shadow zone denotes the location of Ceboruco-San Pedro graben. (*Inset*) Location map of the study area within the North American continent. b) Simplified geologic map of Ceboruco Volcano with structural lineaments (lithologic units after de Ferrari et al., 2003; Sieron and Siebe, 2008). The Post-caldera lavas subdivision follows Nelson (1986). c) Schematic timeline of the eruptive episodes of Ceboruco Volcano (after Böhnel et al., 2016; Sieron et al., 2019).

caldera (Fig. 1*b*), as well as seismic activity (Sánchez et al., 2009; Rodríguez-Uribe et al., 2013; Núñez-Cornú et al., 2020).

Based on the eruptive episodes and periods that Ceboruco Volcano has presented throughout history (Fig. 1*c*), together with the growing population, increasing socio-economic activities, and communication routes in the region near the volcano (Martínez-Álvarez, 2019), the volcanic hazard of Ceboruco is arguably one of the most critical in the country (Suárez-Plascencia, 1998; Sieron et al., 2019), supporting an imperative to monitor and study this volcano.

Mitigating the risk of a potential eruption is one of the civil authorities' interests around the world's volcanic areas; however, it is not always possible to forecast when a volcanic eruption will occur. The forecasting difficulties are mainly related to a lack of knowledge for the volcano in question. Long-term monitoring of volcanoes worldwide

has demonstrated that seismicity can be a powerful tool to infer ongoing processes at volcanoes (White and McCausland, 2016, 2019). These studies show that reactivation of dormant stratovolcanoes after long periods of comparative quiescence is often preceded by volcano-tectonic seismicity (VT) within the distal tectonic fault systems around the volcano. Determining general patterns of seismicity and their underlying mechanisms (Chouet and Matoza, 2013), as well as their evolution over time from long-term data sets, real-time monitoring, and particular knowledge of the volcano affords the potential to generate realistic short-term forecasts regarding the likelihood of an eruption.

Over the last 20 years, seismic monitoring of Ceboruco has been discontinuous, with temporary networks of one and four stations providing general characteristics of seismicity in the vicinity of the volcano. This sparse information, inadequate for establishing a baseline for the current state of the volcano, motivated the installation of a dense temporary seismic network of 25 stations covering an area of 16 × 16 km in the vicinity of the volcano. The main objectives of this deployment were to identify and characterize seismicity and microseismicity in the region and establish various local volcanic seismic origins as well as those arising from regional and local tectonic stresses, classify event types, determine focal mechanisms, and corroborate the occurrence of seismic swarms. The results of this study will be extending our knowledge of the volcano and contribute to an assessment of the potential risk it represents. The enhanced network has improved the earlier event detection threshold, allowed for better location accuracy, permitted the first determination of associated focal mechanisms, and highlighted the need to install a permanent local seismic network. Long-term and continuous data generated by a permanent network would allow the application of more advanced methods for detailing internal volcanic structures and tracking displacements of magmatic fluids that could lead to a volcanic eruption.

2. Regional tectonic and seismic setting

2.1. Tectonic background

The subduction of the Cocos and Rivera Plates beneath the North American Plate controls the complex tectonic processes that occur in the western region of Mexico (Fig. 1*a*). The interaction between these plates gives rise to both the local seismicity and the Trans-Mexican Volcanic Belt (TMVB), which has an oblique orientation to the Middle America Trench. Ceboruco Volcano is located in the western section of the TMVB and is the largest among the numerous volcanoes along the Tepic Zacoalco rift (TZR).

The tectonic environment of the TZR is mainly extensional and, together with the Sierra Madre Occidental, is part of the TMVB (Fig. 1*a*). Some authors proposed an extensional regime with a right-lateral component (Nieto-Obregón et al., 1985; Rodríguez-Castañeda and Rodríguez-Torres, 1992; Petrone et al., 2006; Duque-Trujillo et al., 2014). In contrast, Ferrari et al. (2005) suggested an extensional regime with a left-lateral component. Although it is uncertain if the lateral component is to the right or the left, there is evidence of accommodation zones (Ferrari et al., 2005). Some authors (Nieto-Obregón et al., 1985; Ferrari et al., 2012; Duque-Trujillo et al., 2014) propose the existence of fault systems with NS, NNW-SSE, EW, and ENE-WSW orientations that may have arisen through the complex tectonic history of the study area.

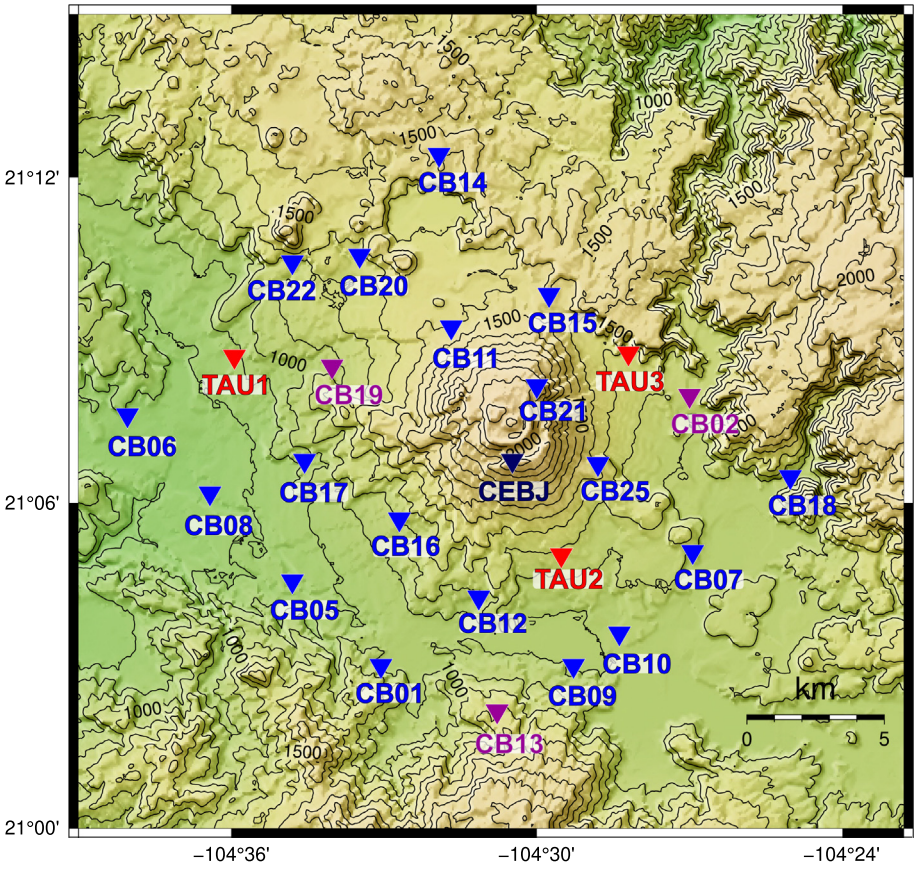

Fig. 2. Station deployment of the Ceboruco Temporary Seismic Network. Purple stations correspond to stations used for cross-correlation; the dark blue station is CEBJ from the RESAJ seismic network. Blue, purple and dark blue stations depict the seismic stations used for this study, while the red inverted triangles were not used. (For interpretation of the references to color in this figure legend, the reader is referred to the web version of this article.)

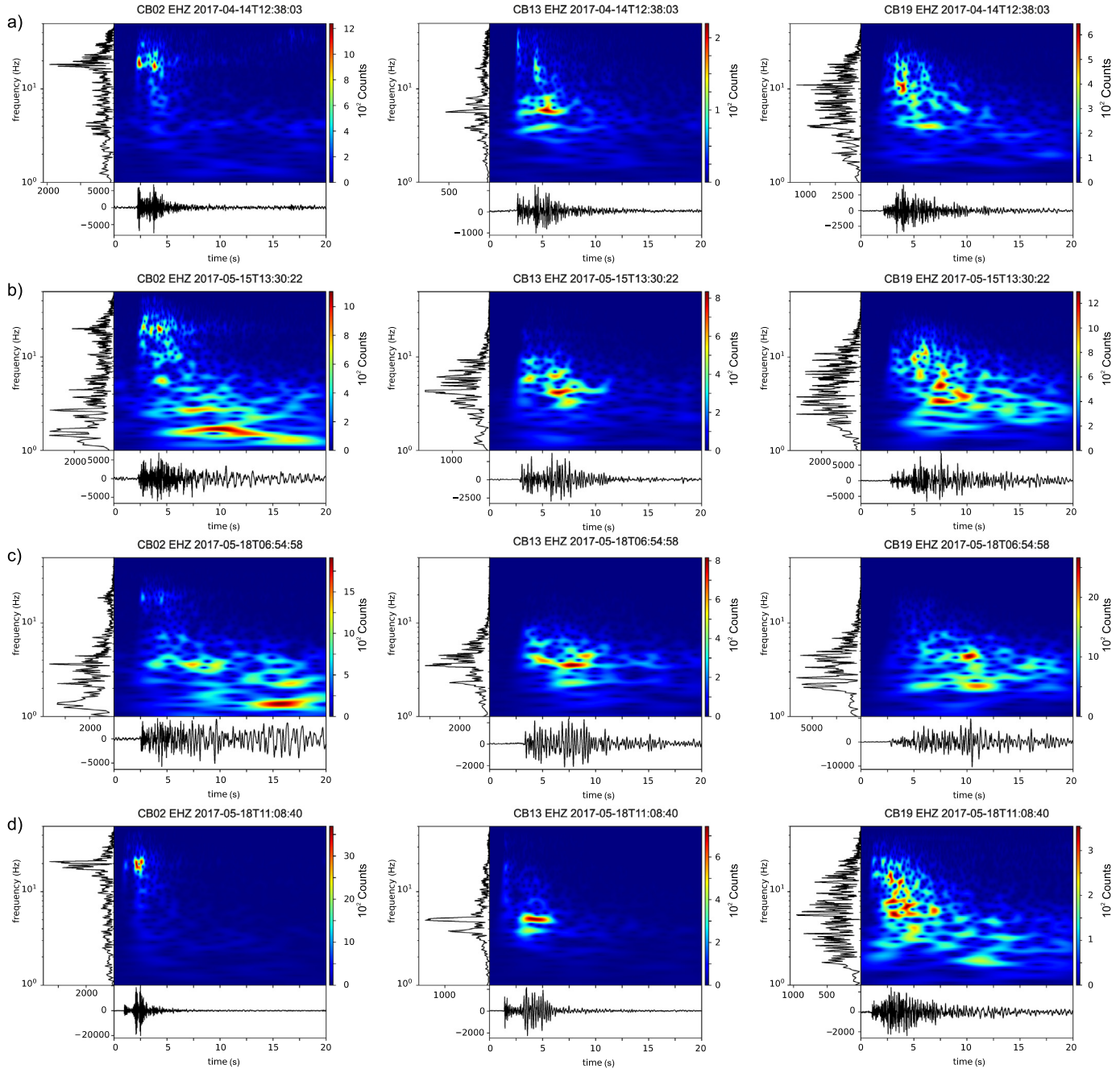

Fig. 3. Seismic signals and spectra of templates used for cross-correlation in this study. Events occurred on a) 2017/04/14 (104) at 12:38 h, b) 2017/05/15 (135) at 13:30 h, c) 2017/05/18 (138) at 06:54 h, and d) 2017/05/18 (138) at 11:08 h observed by CB02, CB13 and CB19 seismic stations (purple triangles of Fig. 2), respectively. (For interpretation of the references to color in this figure legend, the reader is referred to the web version of this article.)

Ceboruco Volcano, together with Tepetiltic Volcano, near the San Pedro Complex, intersect the North Volcanic Chain of the Ceboruco-San Pedro graben (Fig. 1*a*). This is a sub-structure of the TZR, whose opening occurred in several stages and may have initiated 8.5 Ma ago based on the existence of late Miocene basalts at the bottom of the Ceboruco graben (Ferrari et al., 2003). This extensional regime, characterized by a variety of magmas, hosts a monogenetic field composed of scoria cones and domes aligned north and south of the edge of the graben (Northern and Southern Volcanic Chains) (Petrone, 2010). In the vicinity of Ceboruco, the local structures exhibit two preferential trends, NW-SE, similar to the trend of the TZR and associated with its origin, and an ENE-WSW trend that transects the volcano and passes through the crater (Núñez-Cornú et al., 2020) (Fig. 1*b*). These fault systems intersect in the study area and may provide the zone of weakness capable of generating upward movement of magma, and the formation of Ceboruco Volcano. These fault systems have hosted seismicity, suggesting changes in the local stress regime or fluid movement (Sánchez et al., 2009).

Geologically, the current litho-stratigraphic regions are divided into eight units (Fig. 1*b*) which reflect the lavas' geochemical affinity and their association with the change in the tectonic regime (Ferrari et al., 2003; Sieron and Siebe, 2008). The oldest dated lithological unit, the Jala unit, is comprised of ignimbrites and rhyolites, ranging from 4.9 to 4.1 Ma. More recently, the Marquezado tuff (1000 yr) was extruded in the form of domes extending throughout the southern flank of the volcano. The most recent units are the Post-caldera lavas, including the most recent deposits of the 1870 lava flow (Fig. 1*b*).

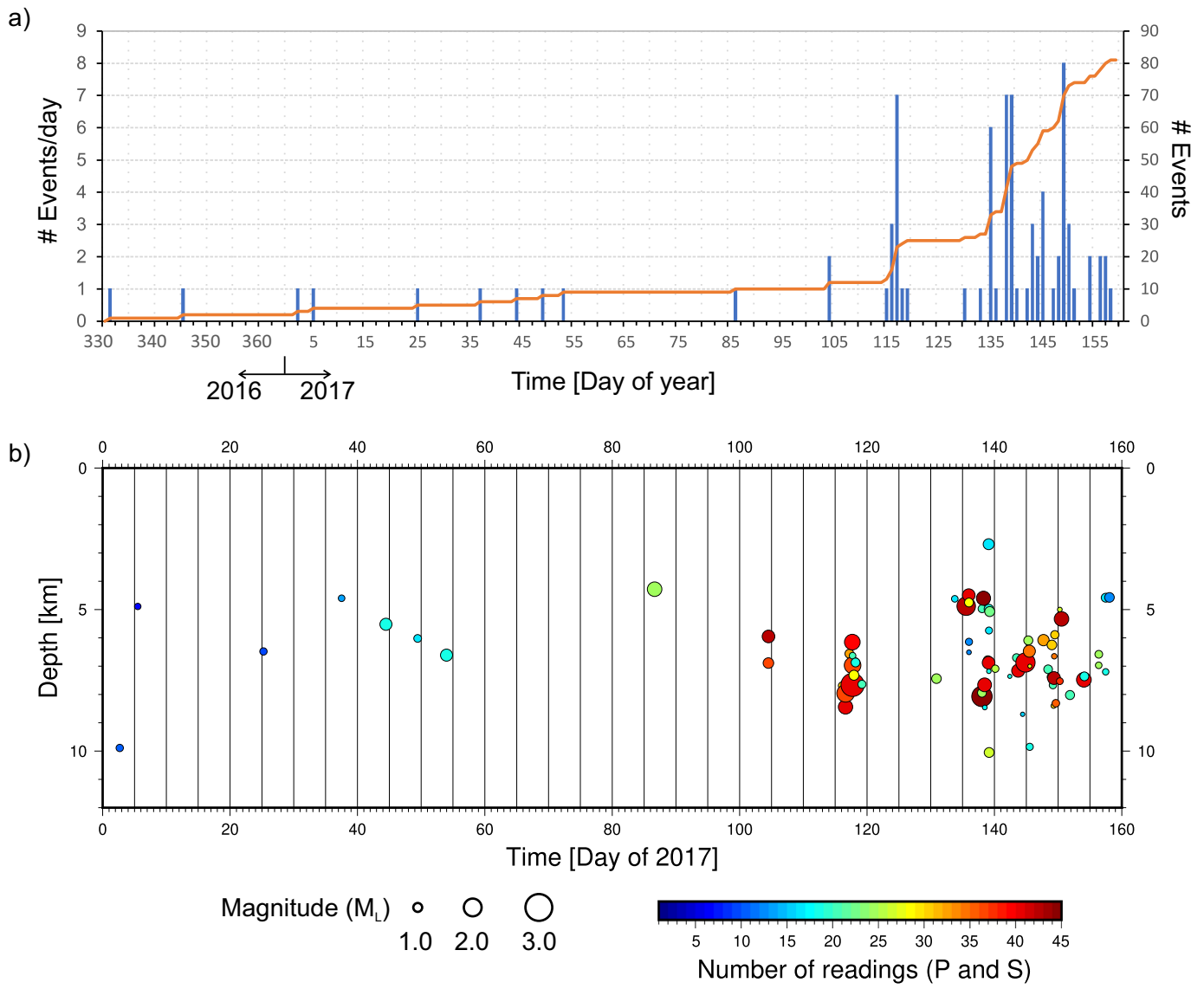

Fig. 4. a) Number of detected events per day from November 27 (332), 2016, to June 7 (158), 2017. The orange line and right y-axis denote the cumulative number of events for the study period. b) Depth section in time with number of P and S wave readings used for each earthquake.

2.2. Volcano-seismicity background

Ceboruco Volcano seismicity studies began more than 25 years ago through various research projects that deployed temporary seismic networks for short time periods and consisted of a small number of stations (Nava et al., 1997; Núñez-Cornú et al., 2002). In 2002 a collaboration agreement was signed between the Research Group CA-UDG-276 Sismología y Volcanología de Occidente (SisVOc) and Nayarit State Civil Defense Department for the installation of a semi-permanent seismic station on the Ceboruco Volcano (CEBN). This station operated intermittently until 2009, when the theft of batteries and solar panels ended data acquisition. From the data generated by CEBN, the fundamental characteristics of the volcano's seismicity could be established. Sánchez et al. (2009) classified observed events as volcano-tectonic (VT), low frequency (LF), and hybrid, according to the terminology proposed by McNutt (1996) (Fig. S1*a*, Supplementary Material). Of the events found, distances for VT-type events were estimated, finding that they were distributed within a 6 km radius of CEBN. Rodríguez-Uribe et al. (2013) used the same database to subclassify LF earthquakes into four types according to their waveform and frequency content: i) Short Duration (Type I), Extended Coda (Type II), Bobbin (Type III), and Modulated Amplitude (Type IV) (Fig. S1*b*, Supplementary Material). These events were distributed randomly within a radius of 9 km from the station. Motivated by the results obtained with a single station, SisVOc installed a temporary seismic network in 2012 made up of three new seismic stations and the reinstallation of CEBN. From the data generated by this seismic network, Núñez-Cornú et al. (2020) establish that volcanic seismicity is mainly related to the structural features of the volcanic edifice and reactivated tectonic structures with ENE-WSW orientation with no obvious hypocentral location pattern for the different types of events found (Fig. S1*c*, Supplementary Material).

3. Seismic data and methods

The seismic data presented in this work were recorded from November 2016 to July 2017 in the vicinity of Ceboruco Volcano, as a part of the strategic project of Centro Mexicano de Innovación en Energía Geotérmica (CeMIEGeo) denoted as P-24 "Passive seismic and magnetotelluric exploration of the Ceboruco Volcano and the La Primavera caldera geothermal fields".

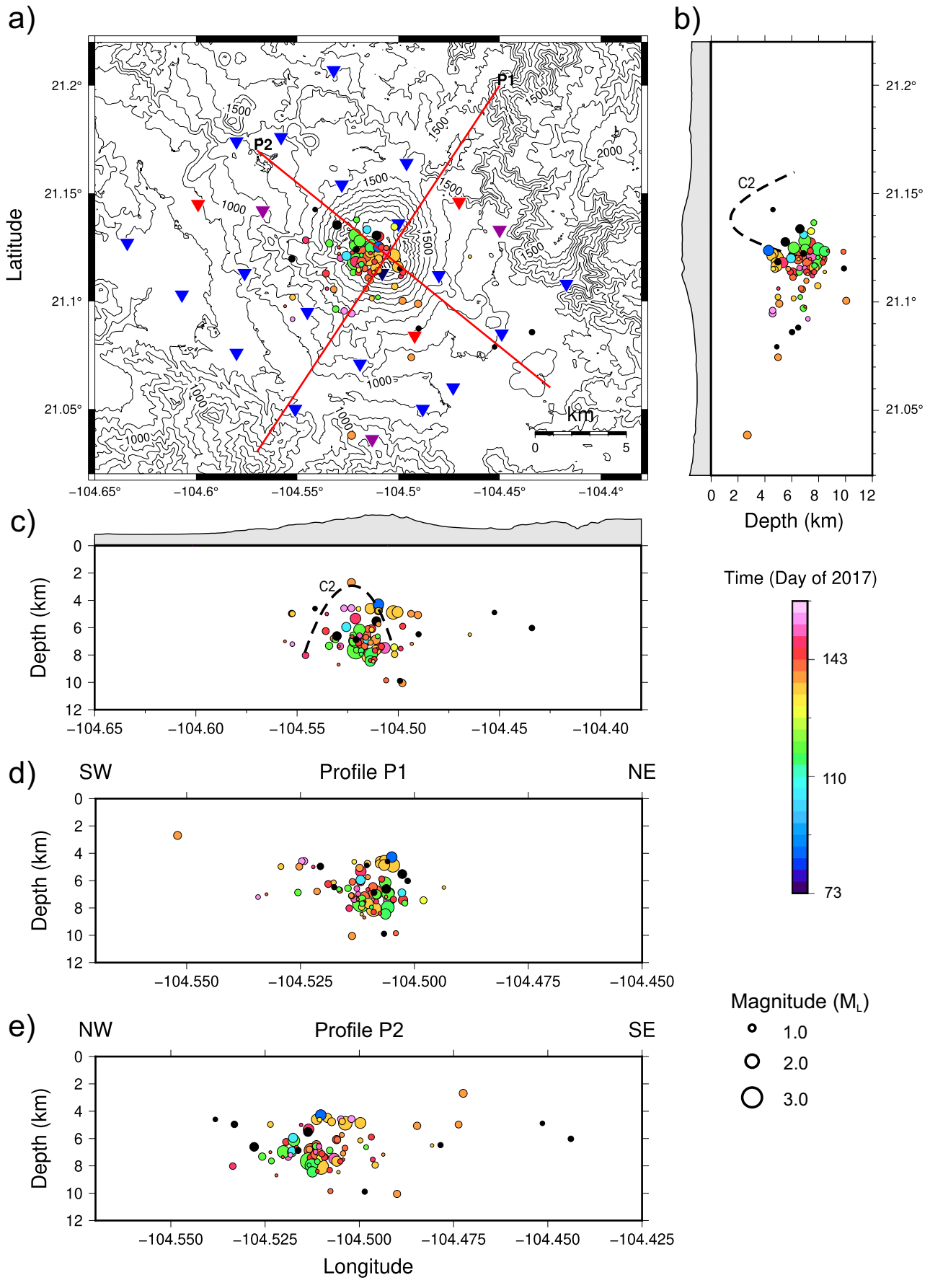
a)
b)
c)
d)
e)
Latitude
Depth (km)
Longitude
P1
P2
C2
km
SW
NW
NE
SE
Profile P1
Profile P2
Time (Day of 2017)
143
110
73
Magnitude (M_L)
1.0
2.0
3.0

3.1. Data acquisition

During the experiment, 21 portable seismic stations were deployed to augment the semi-permanent seismic stations, which had been operating since 2012, and CEBJ, a telemetered seismic station belonging to the Jalisco Seismic Accelerometric Telemetric Network (RESAJ, acronym in Spanish) (Núñez-Cornú et al., 2018). This array provided a dense temporary seismic network of 25 instruments with an average interstation distance of 2–3 km, covering an area of 16×16 km^2 (Fig. 2). The 21 portable seismic stations were each equipped with an Obsidian 4×/8× multichannel seismic recorder (Kinemetrics) and one Lennartz 3D Lite 1 Hz sensor. CEBJ has a Quanterra Q330-6ch Digital Acquisition System digitizer, one Lennartz 3D Lite sensor, and an ES-T Kinemetrics episensor triaxial accelerometer. Each semi-permanent seismic station comprised a Taurus Portable Seismograph digitizer (Nanometrics) and one Lennartz 3D Lite 1 Hz sensor. All stations recorded at 100 samples per second (sps) and 200 sps for the CEBJ accelerometer.

The installation process was conducted in two stages: i) mid-November-early December 2016 with the deployment of 5 stations and ii) February–March 2017 for the others (Fig. S2, Supplementary Material). Simultaneously, Ceboruco magnetotelluric data were being acquired at the end of November 2016, but the theft of some equipment prompted us to suspend both studies until better security was arranged. The deployment resumed in February 2017.

3.2. Seismic data analysis

A database was generated with the seismic records obtained by 25 seismic stations of the Ceboruco dense temporary network using the Antelope software (Lindquist et al., 2007), which automatically performs pre-processing steps, including removal of instrumental response and de-meaning. First, automatic detections were identified using the Antelope system through a short-term average (STA)/long-term average (LTA) signal energy algorithm with an STA window of 1.0 s and LTA window of 30.0 s, with detections in at least four stations. We then manually reviewed the continuous records and picked the P-waves on the vertical component and the S-waves on the horizontal components. Earthquake locations were calculated using the Antelope system and iasp91 velocity model. We selected 56 earthquakes within the region (21.0°, 21.2°) N and (−104.65°, −104.40°) W. A review of waveforms for located events (Fig. S3, Supplementary material) revealed that many shared similar waveforms. We used the cross-correlation detector function of ObsPy (Beyreuther et al., 2010; Megies et al., 2011; Krischer et al., 2015) to assess the similarity between our continuous signals. Four different high-quality waveform templates, extracted from stations CB02, CB13, and CB19 (Fig. 2), were selected based on signal/noise ratio and azimuthal coverage to detect similar or low magnitude events (Fig. 3). Our continuous data scan was conducted applying a 1–15 Hz band-pass filter, a similarity coefficient > 0.75 and a temporal distance between two detections of 10 s to eliminate the possibility of redundancy. We found 25 new events via correlation that were added to our catalog, providing 81 earthquakes. We also calculated local magnitudes (M_L).

Our final catalog (Fig. 4, Figure 5) was relocated using Hypo71PC (Lee and Valdés, 1985) with the same P-wave velocity model used by Núñez-Cornú et al. (2020) (Fig. S4*a*, Supplementary Material). The criteria applied to select the better relocation were: root-mean-square (RMS) arrival time error < 0.5 s, epicentral and depth errors (ERH and ERZ, respectively) < 5.0 km, using seven different starting depths to avoid local minima (1, 3, 7, 10, 12, 15 and 20 km) (Fig. S4*b*, Supplementary Material).

Table 1
Hypocentral distribution of recorded events during the study period.

Depth Intervals (km)	Number of Events	%
[0–4)	1	1.2
[4–6)	22	27.2
[6–8)	48	59.3
[8–10)	9	11.1
> 10	1	1.2

We present the first Ceboruco Volcano focal mechanisms (Fig. 6). Despite the number of stations used in this work, we chose to calculate composite solutions of the focal mechanisms, under the assumption that it is more appropriate in studies of microearthquake activity in confined active regions where the tectonic complexity is elevated (Udías and Buforn, 1980). Application of this method in regional studies allows classification of the mechanisms for a regional solution.

We select those events exhibiting ten or more discernable polarities to evaluate their focal mechanism. The fault plane solution, strike, dip, and slip data were used to calculate the orientation of the principal stresses using first motion direction of P-waves in the Ceboruco Volcano region. We applied the method developed by Brillinger et al. (1980) modified in the MEC93 code by Núñez-Cornú and Sánchez-Mora (1999), in which a probability approach is used to achieve the best solution. Using the output generated by Hypo71PC, this program calculates the fault plane orientation from the first motions of P-waves, adjusting the pressure (P) and tension (T) axes to the observations. MEC93 also calculates the slip, dip, and strike of both nodal planes, the T and P axes directions, and the statistical uncertainty of each parameter (Fig. 6). As a measure of the fit of an observation set, this program uses a score (p) that establishes the proportion of the correct readings comparing theoretical and observed polarities of first motion (Brillinger et al., 1980).

4. Results

4.1. 4.1 Spatio-temporal distribution of Ceboruco microearthquake seismicity

During the experiment, 81 events were detected within the study area (Fig. 4*a*), whose numbers of P and S wave readings used for each event is shown in Fig. 4*b*. The hypocentral and temporal distributions are shown in Fig. 5 and Table 1. Of the total number of events, 48 earthquakes (59.3%) occurred between depths of 6 and 8 km, while 23 shallower events comprised 28.4% of the catalog, and those deeper than 8 km make up the remaining 12.3%. Only one event was deeper than 10 km. In the profiles shown in Fig. 5, we demonstrate that several events occurred synchronously and at similar depths, fitting the definition of seismic swarms. Magnitudes were calculated for 64 earthquakes (79%) of our catalog, obtaining values between $0.5 \le M_L \le 1.5$, while 14 events (17.2%) have magnitudes greater than 1.5 (Table 2). Only four events have $M_L > 2.0$ (Fig. S3, Supplementary material). The largest event, with $M_L = 2.6$, occurred on April 27, 2017, at 5:41 p.m. (Fig. S3*a*). In Fig. 5*a*, a temporal migration of the seismicity from NW to SE (Fig. 5*e*) is exhibited, and a depth migration from 8 km to 4 km (Fig. 5*c*). The epicentral and depth errors obtained in the relocation process show that 75 (93%) events have ERH < 2.0 km while 59 (73%) of 81 total events have ERZ < 2.0 km. The RMS travel-time error is the

Fig. 5. a) Seismicity recorded during this study with P1, and P2 profiles drawn. Circle sizes scale by magnitudes, while color denotes occurrence time according to the day-of-year. b) Seismicity projected along latitude; c) Seismicity projected along longitude. Over b) and c), topographic profiles are depicted. d), and e) correspond to depth sections of P1 and P2 profiles along SW-NE and NW-SE orientations, respectively. Dashed lines show the position of the conductive anomaly C2 proposed by Fuentes-Arreazola et al., (2021). Inverted triangles represent seismic stations, according to Fig. 2.

Table 2
Magnitude distribution of recorded events during the study period.

Magnitude Intervals	Number of Events	%
[0–0.5)	3	3.7
[0.5–1.0)	35	43.2
[1.0–1.5)	29	35.8
[1.5–2.0)	10	12.3
> 2.0	4	4.9

majority in the range of 0.4 s to 0.49 s with 53 (65%) events and 32.5% (26) of the events have RMS < 0.4 s (Fig. S4*b*, Supplementary Material).

4.2. Focal mechanisms determination

Five composite focal mechanisms were obtained (Fig. 6), whose spatial distribution is shown in Fig. 7 and their temporal and depth distribution in Fig. 8. Most focal mechanisms solutions correspond to reverse faults (*a2d*), reverse with strike-slip component (*a1c*), and oblique faults (*a2j*) and are mainly located inside the volcano edifice with N-S preferential orientations (Fig. 7*a*). The normal faults (*a2k*) show an NW-SE preferential tendency, parallel to the orientation of the TZR (Fig. 7*b*). The strike-slip focal mechanisms obtained are situated at the edge of the volcanic structure and could be associated with pre-existing tectonic faults (Fig. 7*c*).

The occurrence in time and depth of the events associated with focal mechanisms shows most of them occurred between Julian days 115 and 159 (Fig. 8) and in a depth range of 5–10 km. We observe four seismic sequences during this period (Fig. 9): I (115–118 Julian days), II (135–140 Julian days), III (143–145 Julian days), and IV (147–150 Julian days). Sequence I (Fig. 8*b*, 9*a*) is composed of 13 events. The first nine events are spatially aligned in the N-S direction west of the volcano summit. Sequence II (19 events) is characterized by pure reverse focal mechanisms located in the southern sector of the volcanic edifice (Fig. 8*c*, 9*b*), followed three days later by sequence III (8 earthquakes), whose normal fault mechanisms exhibit nodal planes oblique to the S–N linear migration direction of the hypocenters (Fig. 8*c*, 9*c*). This could indicate the presence of en-echelon extensional cracks related to the general regional stresses. Sequence IV comprises 15 seismic events whose epicentral distribution is mainly NW-SE (Fig. 8*c*, 9*d*).

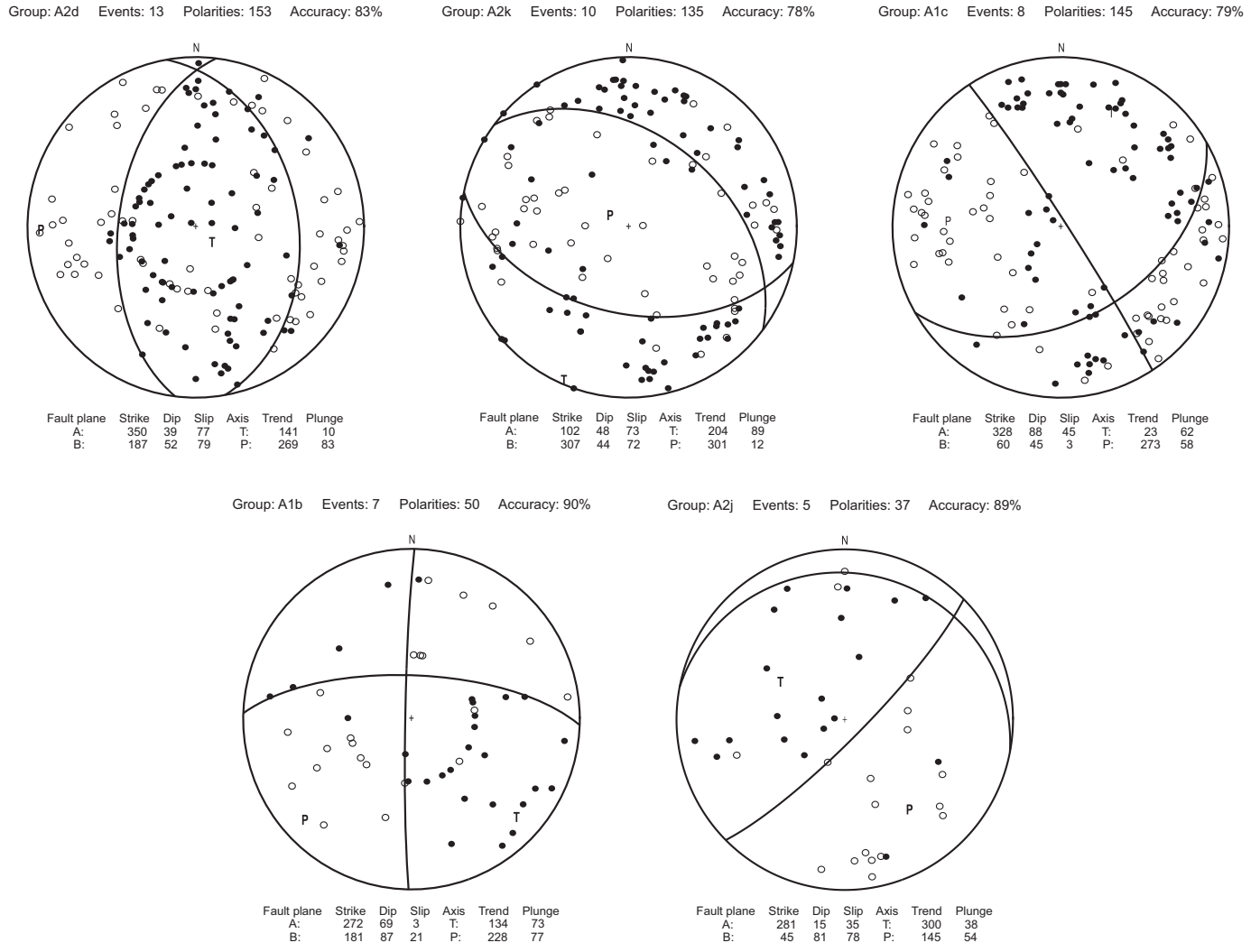

Fig. 6. Stereographic projection of the solutions obtained for our seismic catalog with the number of used events, focal planes, T and P axis, and score *p* (%). Black dots represent compression first motion, whereas empty circles represent dilatational first motion.

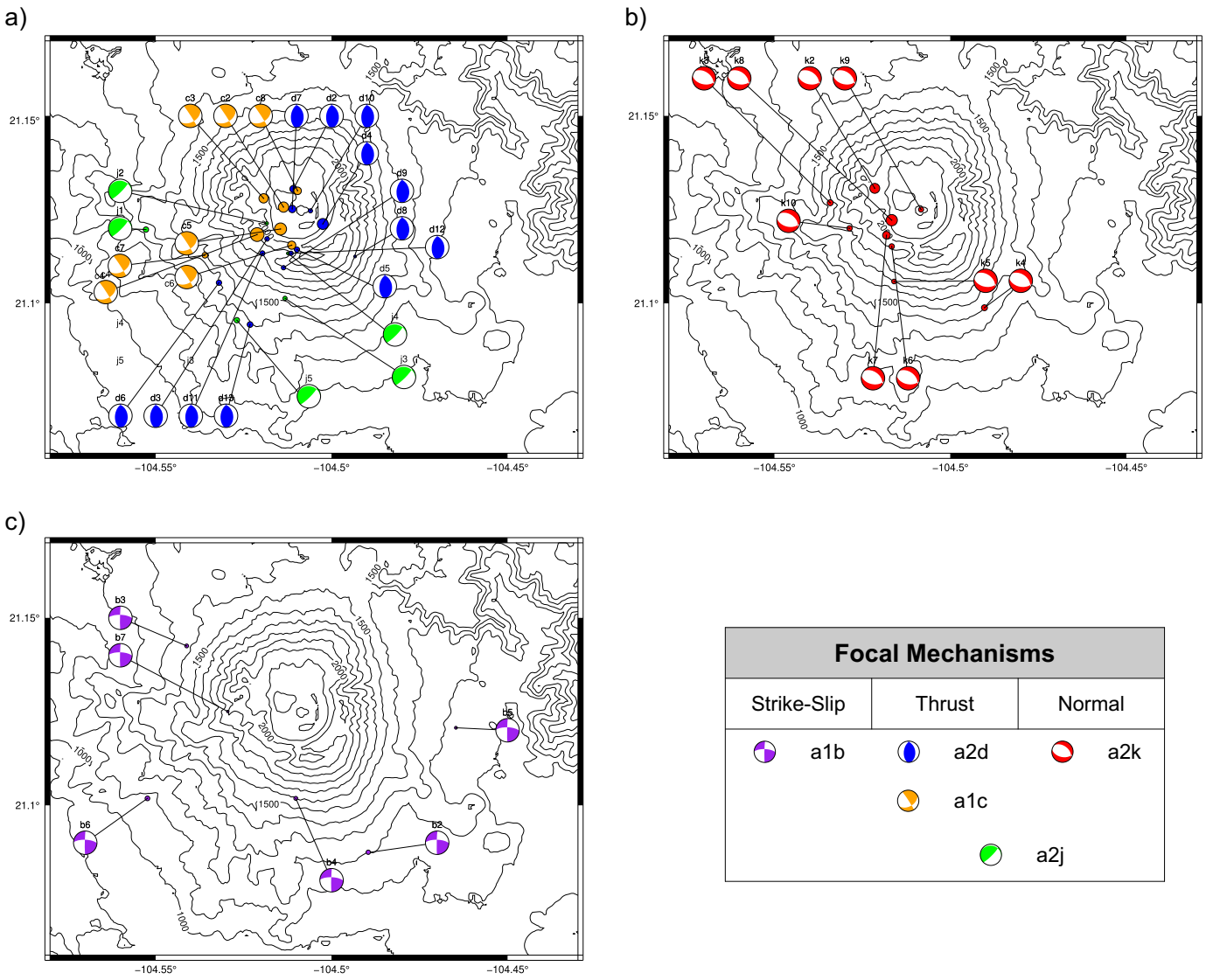

Fig. 7. Seismic events with composite focal mechanisms. Circle sizes scale by magnitudes, while color denotes the associated mechanism. a) Reverse (*a2d*), reverse with strike-slip component (*a1c*) and oblique (*a2j*) solutions; b) Normal (*a2k*) solutions; c) Strike-slip (*a1b*) solutions.

The resulting mechanisms calculated in this sequence have a mainly reverse fault component.

4.3. Seismic signal classification

Following Ceboruco Volcano seismicity classification schemes by Sánchez et al. (2009), Rodríguez-Uribe et al. (2013), and Núñez-Cornú et al. (2020), we classified the events of our catalog into hybrid and low-frequency types. Low-frequency events (LF), in turn, have been subclassified into Type I or Short Duration events (Figs. 10*a, a'*), Type II or Extended Coda (Figs. 10*b, b'*), and Type IV or Modulated Amplitude earthquakes (Figs. 10*c, c'*), according to the classification made by Rodríguez-Uribe et al. (2013). Hybrid events (Figs. 10*d, d'*) are characterized by high-frequency onsets and low-frequency codas with spectral contents of approximately 2 to 10 Hz. In Fig. 11*a*, we observe the spatial distribution of these types where the Hybrid events are aligned in a NW-SE direction, while Type I and II events are located within the volcano, and Type IV events are distributed more broadly in the area surrounding the volcano. In Figs. 11*b, c,* and *d*, we observe their temporal and depth distribution, where the Hybrid events occurred mainly between Julian days 143 and 157 and within a depth range of 5 to 8 km. The LF Type I and II events usually occur in very close periods and depths. Although Type IV events appear to be observed in simultaneous periods, their depths are more variable.

5. Discussion

The analysis of new seismic data, obtained through the dense temporary network installed during the P-24 project of the CeMIEGeo, provides us a detailed distribution of seismic activity in the Ceboruco Volcano region and its relationship with the main tectonic structures.

Previous seismicity studies at Ceboruco Volcano revealed that earthquakes occurred mainly on the faults near the volcano. Those studies were carried out with a single seismic station, CEBN, where the presence of VT-type, low-frequency and hybrid events was observed (Sánchez et al., 2009; Rodríguez-Uribe et al., 2013). Most of the VT events were epicentrally distributed within a radius of 5 km from CEBN. In comparison, the low-frequency events were randomly distributed within a

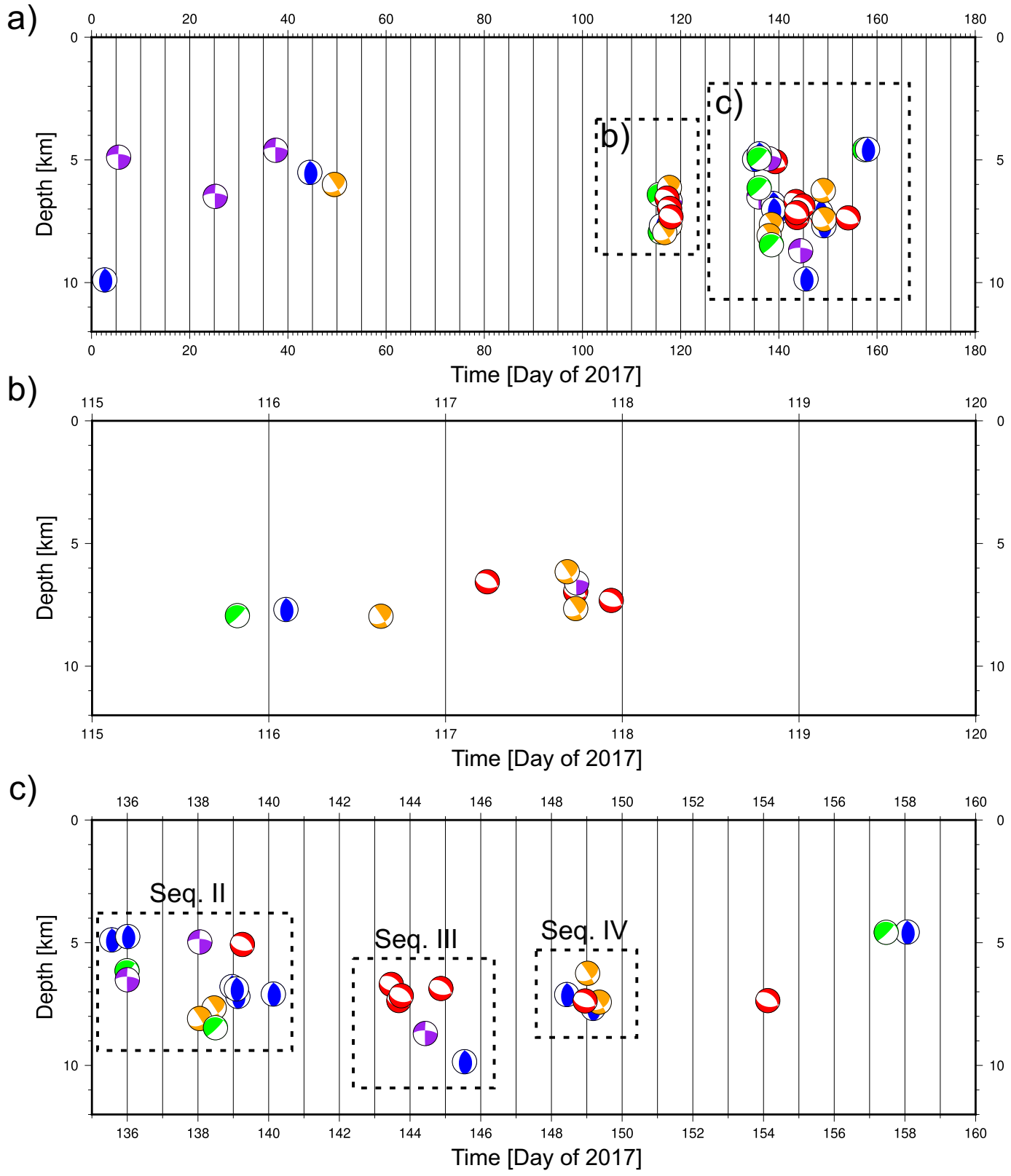

Fig. 8. a) Depth section in time with focal mechanisms. Dash-lined rectangles denote enlargements corresponding to the sections shown in b) and c). b) Depth section in time for days 115–120, 2017. c) Depth section in time for days 135–160, 2017.

radius of 9 km from CEBN with no clear distribution pattern according to the observed families. The installation of three temporary seismic stations and CEBN allowed calculating hypocenters of events recorded in 2012–2014 (Núñez-Cornú et al., 2020). It was observed that the events largely occurred between depths of 0 and 10 km within a radius of 9 km from CEBN, but locations had significant uncertainty. Low-frequency

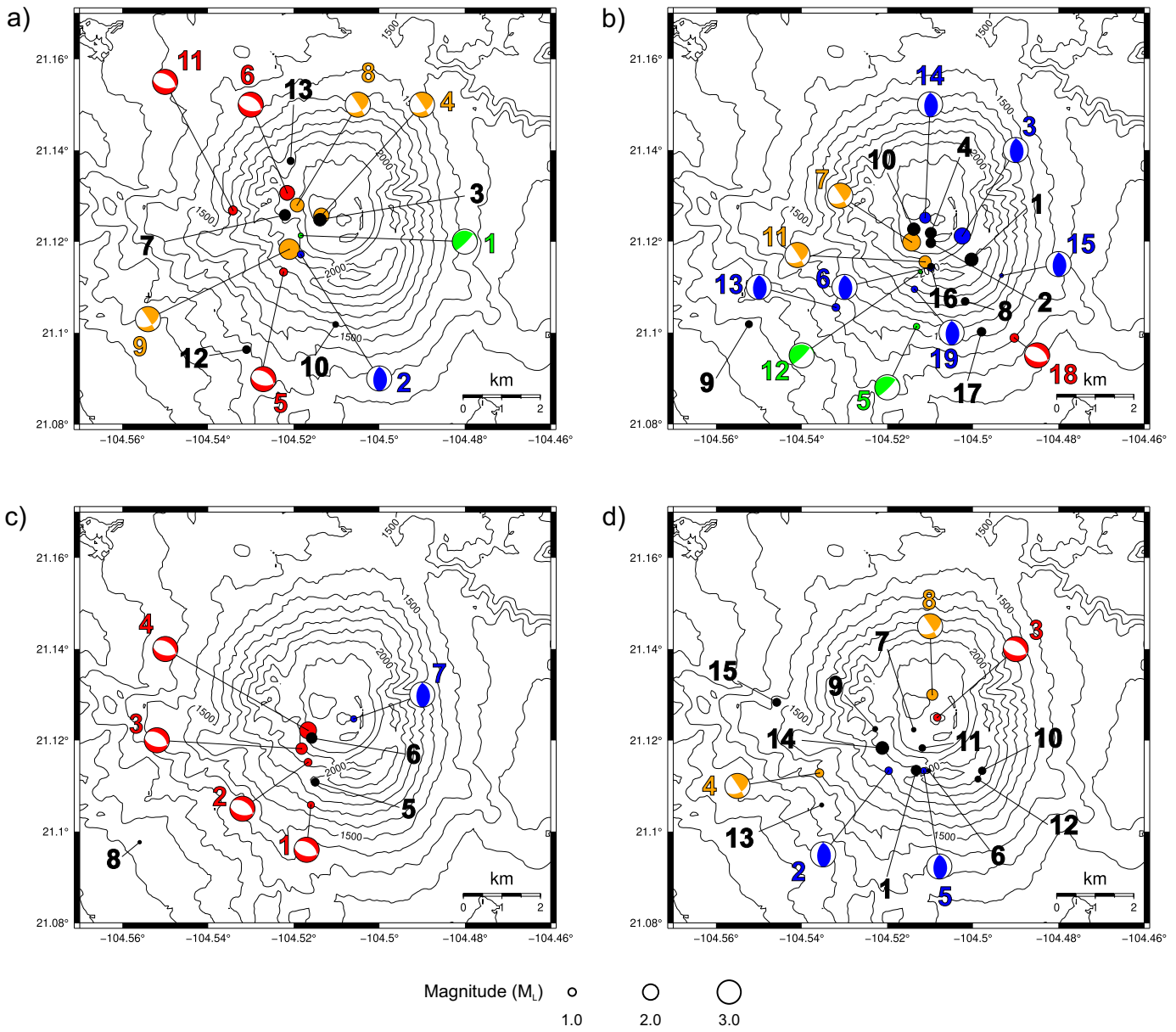

Fig. 9. Seismic sequences occurring during the study period. a) Sequence I (days 115–118, 2017); b) Sequence II (days 135–140, 2017); c) Sequence III (days 143–145, 2017); d) Sequence IV (days 147–150, 2017). Circle sizes scale by magnitudes, while color denotes the associated mechanism. Black circles and numbers show events without associated composite focal mechanisms.

events of type I, II and IV were observed but no swarming or spatial clustering was detected. No VT events were observed in the study period. The epicentral distribution of recorded events showed three alignments coinciding with structural guidelines associated with local and regional stresses, two of which transect the volcanic edifice; the other was located to the SE of the volcano. This seismicity might be related to the movement of magmatic fluids along these structural lineaments.

The analysis of our microseismicity was influenced by the two stages of the installation process. From November 2016 to February 2017, only three seismic stations worked correctly and the other three intermittently (Fig. S2). In this period, only five events were recorded with magnitudes $0.73 < M_L < 1.0$. The remaining stations were installed from February to March, and their operation was adequate from April until the end of June 2017. This is reflected in the quantity and quality of P and S wave readings used for location (Fig. 4*b*). In addition, we can observe that around the 100th day of 2017, most of the events were located with more than 20–25 readings, and those with magnitudes greater than 1.1 with more than 36 readings, so at least 18 stations were able to record them. The small magnitude events were only recorded by stations close to the events and not by the entire network.

In our study, we observed that most of the recorded microearthquake activity occurs within the volcanic edifice, spatially concentrated between the NW and SW region of the volcano and primarily between 6 and 8 km in depth, having magnitudes between M_L 0.5 and 2.6.

We observed a migration from NW to SE and from 8 to 4 km depth (Fig. 4a and c), corresponding to the events that occurred during Sequences I and II. The migration speed from NW to SE has been estimated at 0.12 km/day (almost 3 km laterally in about 24 days), while the shoaling rate is approximately 0.16 km/day (almost 4 km of ascent in about 24 days). During this period the average event rate was 1.52 eq/day, predominantly Type I and II LF events (Fig. 11); these events exhibited both normal and strike-slip focal mechanisms in Sequence I and inverse mechanisms in Sequence II (Figure 9).

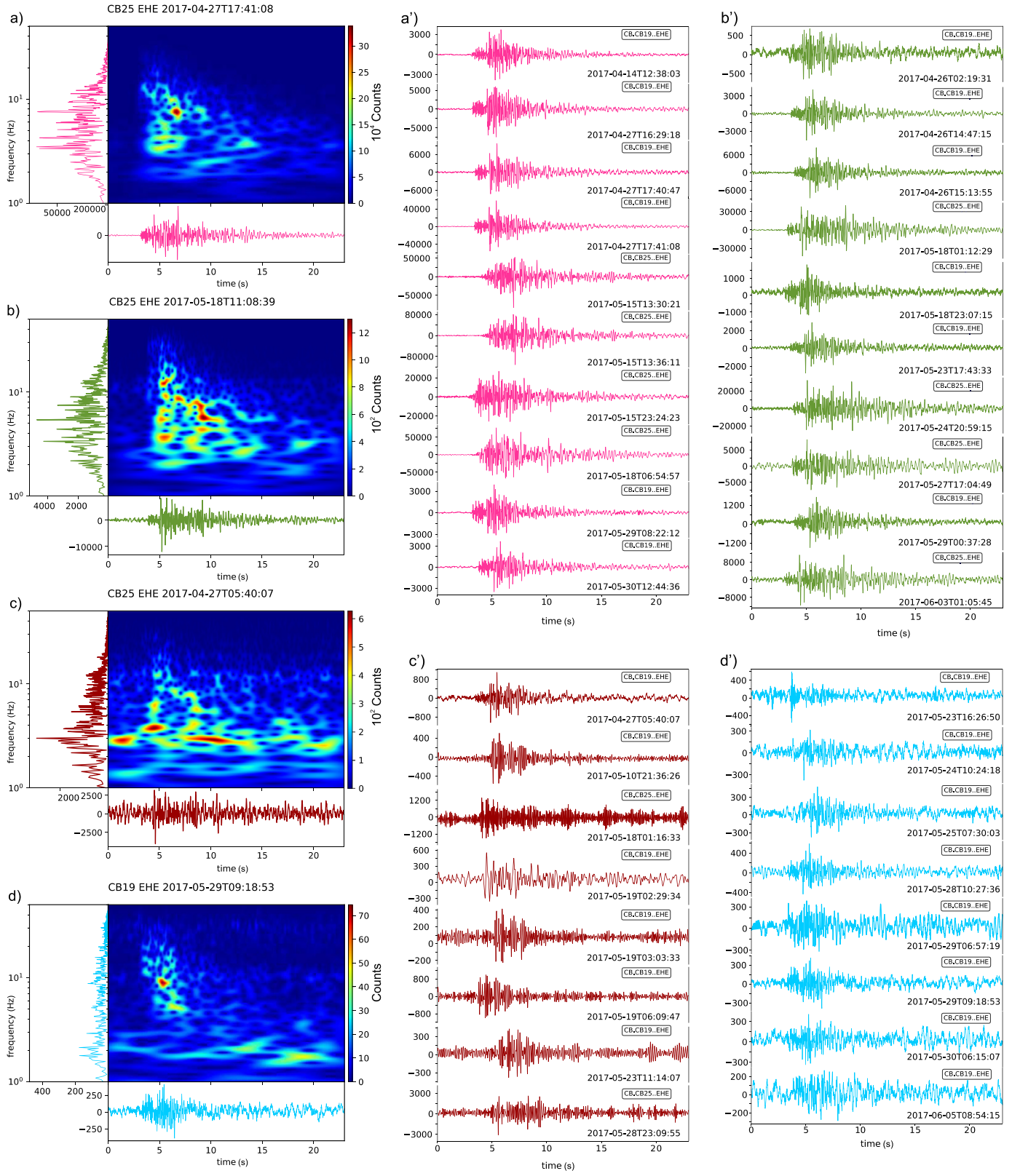

Fig. 10. Spectrograms and seismograms of each type of event detected. a) and a') correspond to Low-Frequency Type I (Short-duration); b) and b') Low-Frequency Type II (Extended Coda); c) and c') Low-Frequency Type IV (Modulated Amplitude) and d) and d') Hybrids (after Sánchez et al., 2009 and Rodríguez-Uribe et al., 2013).

Our study also suggests that a significant part of the low-magnitude seismicity may have been beneath the detection threshold of the temporary networks previously installed. The deployment of the dense temporary network allowed establishing a consistent detection threshold in the area of interest, whose minimum magnitude was 0.4–0.5. It increased the accuracy of hypocentral determinations, obtaining an

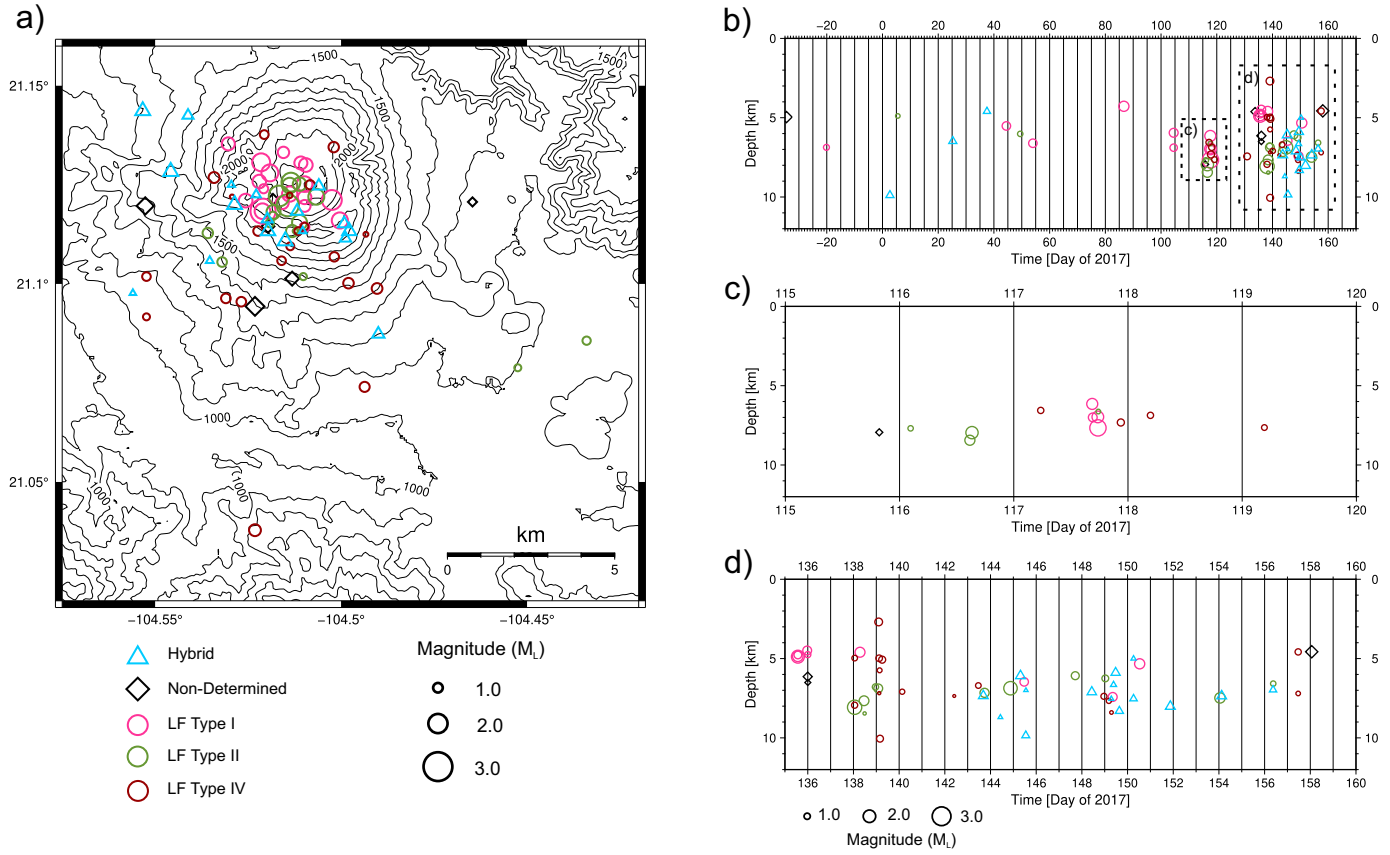

Fig. 11. a) Seismicity classified into types. Symbol sizes scaled by magnitudes. b) Depth section in time with families. Dash-lined rectangles denote enlargements corresponding to the sections shown in c) and d). c) Depth section in time between days 115–120, 2017. d) Depth section in time between days 135–160, 2017.

average ERH and ERZ of 1.1 and 1.3 km (Fig. S4b, Supplementary Material), respectively, a 50% reduction compared to the Núñez-Cornú et al. (2020) values of 2.5 km for 88% of their earthquake locations. We have identified four seismic sequences with an average duration of three days and one that lasted five days (Sequence II, Fig. 9*b*), which provided unambiguous focal mechanisms. Sequence II exhibited mainly reverse faulting.

A diurnal and semidiurnal apparent periodicity of the Ceboruco swarms suggests a tidal influence to triggering the events, and such behavior has been noted at numerous other volcanoes (e.g., Dzurisin (1980); Rydelek et al. (1988); Petrosino et al., 2018; Miguelsanz et al., 2020). Some of the Ceboruco Volcano microseismicity (Sequences I and II) occurred almost exclusively during tidal maxima or minima (Fig. 12*a*, *b*), begging the question of associated crustal stress modifications in a shallow hydrothermal system that is in a state of unstable equilibrium. The short time series and small number of events, however, do not conclusively indicate tidal effects, as other local diurnal influences may be in play. Neuberg (2000) suggests that such observations could indicate shallow perturbations due to daily temperature changes or rainfall, although such effects would seem applicable to only near-surface events, and not those at depths of 2 km and more. Neuberg (2000) also points to the potential for the influence of changing diurnal barometric pressure, which in a warm climate could conceivably perturb an especially gas-rich system. Barometric pumping is a known effect for gas leakage from shallow sources (e.g., Forde et al., 2019) and might control the shallowest fracture mechanics at Ceboruco where fumarolic activity is observed at the surface, but its contribution to system perturbations influencing seismic swarms at depths on the order of 2 km or greater may be negligible. One of the arguments supporting a tidal forcing influence for Ceboruco can be seen in Fig. 12*b*, in which the solar and lunar tidal functions are clearly distinguishable and some events appear associated with both curves; Neuberg (2000) dismissed tidal effects based on the lack of correlation with the lunar curve for the example volcanoes he considered. In short, our data are insufficient to state with certainty what the diurnal influence is, only that we seem to observe one.

The strike-slip fault solutions (*a1b*) are associated with hypocenters located at the edge of the volcano edifice (Fig. 7*c*). One nodal plane indicates a left-lateral mechanism orientated towards the NW-SE (*a1c* and *a1b*), parallel to the TZR. Most of the events correspond to Type I and II LF earthquakes. The lateral movement of the *a2j* group is less clear, and they are located at the southwestern edge of the volcano (Fig. 7*a*). The ENE-WSW right lateral fault solution is oblique to the rift trend and is consistent with the most recent deformation stage in the area. The more modern structures could be related to Riedel R or P shear secondary structures associated with the main faulting.

Inside Ceboruco Volcano, both thrust and normal fault mechanisms are observed. The pure thrust fault solutions (*a2d*) have N-S preferred trend and do not follow the regional deformation pattern, indicating that these faults may be associated with older faults reactivated by the ascent of fluids (Fig. 7*a*); however, the normal fault (*a2k*) trend is NW-SE, parallel to the main orientation of the TZR, whose associated events correspond to modulated amplitude and hybrid types (Figs. 8*b* and 12*a*). Their events and mechanisms are consistent with extensional movement along the rift, as shown by the fault solution orientation and the trend of its extensional axis.

A recent study from 3D inversion modeling of magnetotelluric data (Fuentes-Arreazola et al., 2021) proposes the existence of a conductive anomaly C2 beneath the Ceboruco Volcano summit with resistivity values of 2–5 Ωm, whose interpretation is intriguing and could

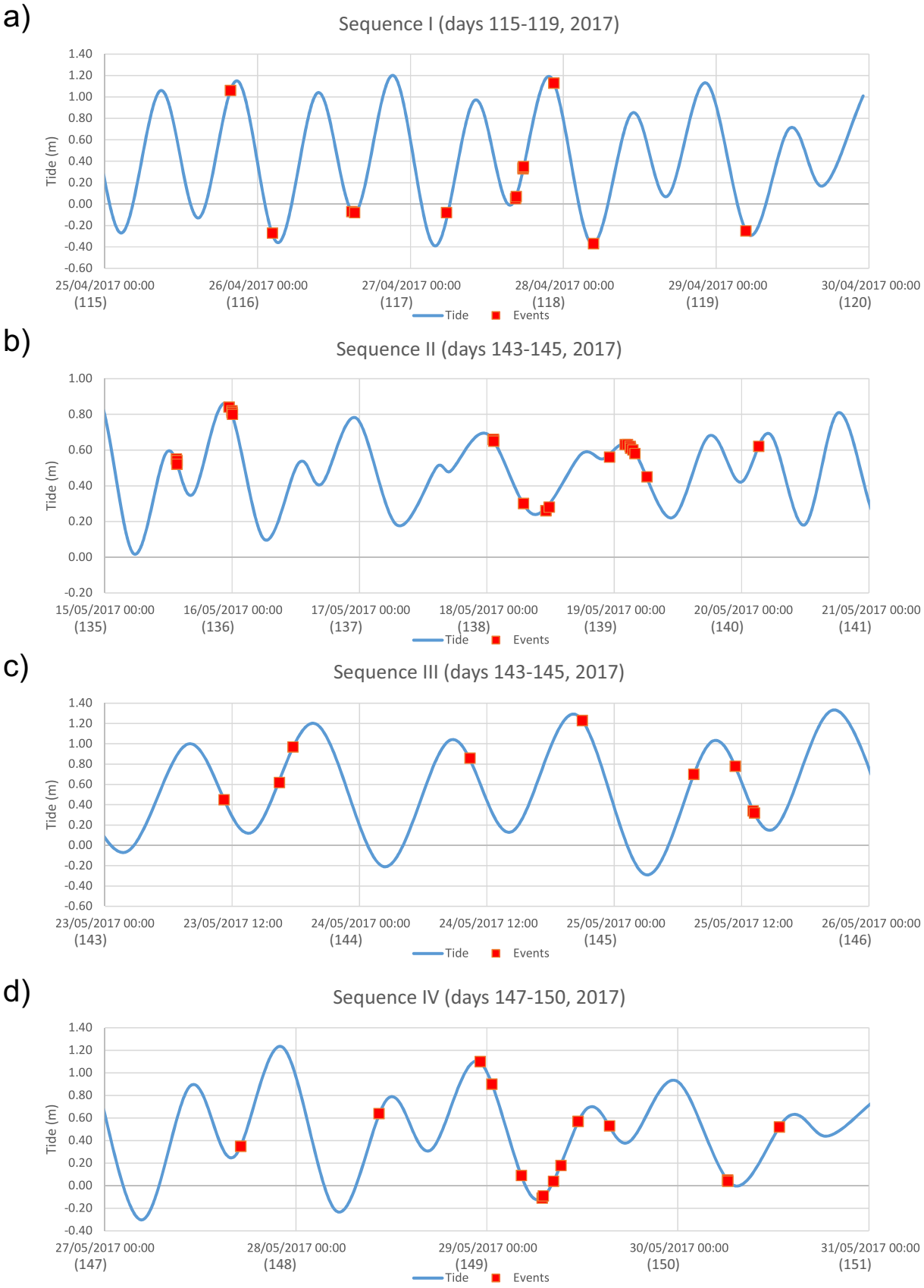

Fig. 12. Correlation between tide and seismic sequence occurrence. a) Sequence I (days 115–118, 2017); b) Sequence II (days 135–140, 2017); c) Sequence III (days 143–145, 2017); d) Sequence IV (days 147–150, 2017). Red squares denote seismic events that occurred during the corresponding sequence. (For interpretation of the references to color in this figure legend, the reader is referred to the web version of this article.)

correspond to a shallow ancient magma chamber enveloped by high-temperature fluids interacting with the host-rocks and hydrothermal system. Most of the seismicity obtained in this study is located in the southwestern region of the C2 anomaly (Fig. 5*b*, *c*), supporting the previous interpretation; however, the events associated with reverse fault mechanisms and the temporal-depth migration from deeper to shallow could indicate compression of ascendant material, implying a possible resumption of the volcano activity.

6. Conclusions

The present study has allowed us to obtain locations for seismicity associated with Ceboruco Volcano, confirming the existence of seismic events associated with the interaction of the volcano system and local tectonics. Most of the events observed in this analysis occur in seismic swarms. This study presents the first detailed analysis of microearthquakes occurring within and adjacent to Ceboruco Volcano. We have observed the occurrence of seismic sequences and temporary migrations from NW to SE and from deeper to shallower hypocentral depths. Furthermore, the different focal mechanisms obtained from our seismicity data provide new insights regarding the local faults that follow the Tepic-Zacoalco rift orientation, but also ancient faults, which are not associated with the current regional deformation pattern and could be exhibiting reactivation by the ascent of magmatic fluids.

These results confirm the necessity of maintaining a permanent seismic network on and around this active volcano to follow in real-time the state of the volcanic system that could allow a short-time forecast. The seismic data provided by a permanent seismic network will allow exploiting in more detail advanced methods for the identification of microearthquakes, tomography methods to improve the knowledge of the internal volcanic structures or define variation in seismic velocities. These studies would allow us to complement the work presented here and clarify the resulting hypotheses.

The documented violent explosive eruptions of Ceboruco Volcano in the past and the significant economic and demographic growth in the area today compels us to conclude that the vulnerability and risk have increased significantly. It is therefore vitally important to understand and document Ceboruco's baseline behavior in order to detect and interpret anomalies in the future properly.

Funding

This research was funded by P24 Project of the Centro Mexicano de Inovación en Energía Geotérmica [CeMIEGeo] of the Secretaría de Energía MEXICO-Consejo Nacional de Ciencia y Tecnología (SENER-CONACyT) 201301-207032. CEBJ seismic station was installed as a part of the RESAJ Project, funded by Consejo Nacional de Ciencia y Tecnología (CONACYT) – FOMIXJAL 2008–96538 (2009) (Mexico). Partially supported under the US Department of Energy Contract 89233218CNA000001

Data and resources

The seismicity data generated for this study are in a database at Research Group 276 Sismología y Volcanología de Occidente (CA-UDG-276 SisVOc). These data are available for collaborative research projects between CA-UDG-276 SisVOc and other interested institutions by specific agreements. For information, contact Francisco J. Núñez Cornú (pacornu77@gmail.com).

Declaration of Competing Interest

The authors declare that they have no known competing financial interests or personal relationships that could have appeared to influence the work reported in this paper.

Acknowledgments

The authors are very grateful to Felipe de Jesús Escalona-Alcázar for his fruitful observations and valuable comments. We thank to the anonymous reviewers for their thorough and thoughtful comments that improved the manuscript significantly. Some figures were generated using the Generic Mapping Tools (GMT-6; Wessel et al., 2019) and ObsPy (Beyreuther et al., 2010; Megies et al., 2011; Krischer et al., 2015). This is Los Alamos National Laboratory Publication number LA-UR-20-27934, partially supported under the US Department of Energy.

Appendix A. Supplementary data

Supplementary data to this article can be found online at https://doi.org/10.1016/j.jvolgeores.2021.107451.

References

Banda, L., 1871. Breves noticias del Volcán del Ceboruco. Boletín de la Sociedad de Geografía y Estadística de la República Mexicana, Segunda época, tomo III, Imprenta del Gobierno en el Palacio de México. pp. 26–34 (In Spanish).

Barrera, T., 1931. Zonas mineras de los estados de Jalisco y Nayarit. Boletín del Instituto Geológico de México 51, 5–46 (In Spanish).

Beyreuther, M., Barsch, R., Krischer, L., Megies, T., Behr, Y., Wassermann, J., 2010. ObsPy: a Python Toolbox for Seismology. Seismo. Res. Lett. 81. https://doi.org/10.1785/gssrl.81.3.530.

Böhnel, H., Pavón-Carrasco, F.J., Sieron, K., Nasser Mahgoub, A., 2016. Palaeomagnetic dating of two recent lava flows from Ceboruco Volcano, western Mexico. Geophys. J. Int. 207 (2), 1203–1215.

Brillinger, D., Udías, A., Bolt, B.A., 1980. A probability model for regional focal mechanism solutions. Bull. Seismol. Soc. Am. 70, 149–170.

Caravantes, A., 1870. El Ceboruco. La Naturaleza, Periódico Científico de la Sociedad Mexicana de Historia Natural, Tomo I, Imprenta de Ignacio Escalante, Mexico. pp. 248–252 (In Spanish).

Chouet, B.A., Matoza, R.S., 2013. A multi-decadal view of seismic methods for detecting precursors of magma movement and eruption. J. Volcanol. Geoth. Res. 252, 108–175.

Duque-Trujillo, J., Ferrari, L., Norini, G., López-Martínez, M., 2014. Miocene faulting in the southwestern Sierra Madre Occidental, Nayarit, México: kinematics and segmentation during the initial rifting of the southern Gulf of California. Rev. Mex. Ciencias Geol. 31, 283–302.

Dzurisin, D., 1980. Influence of fortnightly tides at Kilauea volcano. Hawaii. Geoph. Res. Lett. 7, 925–928.

Ferrari, L., Nelson, S.A., Rosas-Elguera, J., Aguirre-Díaz, G., Venegas-Salgado, S., 1997. Tectonics and volcanism of the western Mexican Volcanic Belt. In: Aguirre-Díaz, G., Aranda-Gómez, J., Carrasco-Núñez, G., Ferrari, L. (Eds.), Magmatism and Tectonics in Central and Northwestern Mexico. Selections of the 1997 IAVCEI General Assembly Excursions. Instituto de Geología, Universidad Nacional Autónoma de México 85–29.

Ferrari, L., Petrone, C.M., Francalanci, L., Tagami, T., Eguchi, M., Conticelli, S., Manetti, P., Venegas-Salgado, S., 2003. Geology of the San Pedro-Ceboruco Graben, western Trans-Mexican Volcanic Belt. Rev. Mex. Ciencias Geol 20, 165–181.

Ferrari, L., Valencia-Moreno, M., Bryan, S., 2005. Magmatismo y tectónica en la Sierra Madre Occidental y su relación con la evolución de la margen Occidental de Norteamérica. Boletín de la Sociedad Geológica Mexicana, LVII, pp. 343–378.

Ferrari, L., Orozco-Esquivel, T., Manea, V., Manea, M., 2012. The dynamic history of the Trans-Mexican Volcanic Belt and the Mexico subduction zone. Tectonophysics 522–523, 122–149.

Forde, O.N., Cahill, A.G., Beckie, R.G., Mayer, K.U., 2019. Barometric-pumping controls fugitive gas emissions from a vadose zone natural gas release. Scientific Reports 9 Article number 14080.

Fuentes-Arreazola, M.A., Núñez, D., Núñez-Cornú, F.J., Calderón-Moctezuma, A., Ruiz Aguilar, D., Romo-Jones, J.M., 2021. Magnetotelluric imaging of the Ceboruco Volcano, Nayarit, Mexico. J. Volcanol. Geoth. Res. https://doi.org/10.1016/j.jvolgeores.2021.107339.

Iglesias, M., 1875. La exploración científica del Ceboruco. Edición oficial, informe y colección de artículos relativos a los fenómenos geológicos verificados en Jalisco en el presente año y en épocas anteriores. Tomo II, tipografía de S. Banda, Guadalajara 354 pp. (In Spanish).

Iglesias, M., Bárcena, M., Matute, J.I., 1877. El Ceboruco. Anales del Ministerio de Fomento de México 1, 168–196 (In Spanish).

Krischer, L., Megies, T., Barsch, R., Beyreuther, M., Lecocq, T., Caudron, C., Wassermann, J., 2015. ObsPy: a bridge for seismology into the scientific Python ecosystem. Comput. Sci. Disc. 8, 014003.

Lee, W.H.K., Valdés, C.M., 1985. HYPO71PC; a personal computer version of the HYPO71 earthquakes location program. U.S. Geol. Surv. Open-File Report. 85-749.

Lindquist, K.G., Newman, R.L., Vernon, F.L., 2007. The antelope interface to PHP applications: web-based real-time monitoring. Seismol. Res. Lett. 78 (6), 663–670. https://doi.org/10.1785/gsrrl.78.663.

Martínez-Álvarez, J., 2019. Zonificación de la vulnerabilidad por actividad del Volcán Ceboruco, Nayarit (México). Master's thesisUniversidad de Guadalajara 149 pp. (In Spanish).

McNutt, S.R., 1996. Seismic monitoring and eruption forecasting of volcanoes: A review of the state-of-the-art and case histories. In: Scarpa, R., Tilling, R. (Eds.), Monitoring and Mitigation of Volcano Hazards. Springer, Berlin, pp. 99–146.
Megies, T., Beyreuther, M., Barsch, R., Krischer, L., Wassermann, J., 2011. ObsPy – what can it do for data centers and observatories? Ann. Geophys. 54 (1), 2011. https://doi.org/10.4401/ag-4838.
Miguelsanz, L., Gonzales, P.J., Tiampo, K.F., Fernandez, J., 2020. Tidal influence on seismic activity during the 2011-2013 El Hierro volcanic unrest. Tectonics 40. https://doi.org/10.1029/2020TC006201.
Nava, F.A., García-Arthur, R., Suárez, C., Márquez, B., Núñez-Cornú, F., Saavedra, G., 1997. Seismic activity at the Ceboruco-Tepetiltic volcanic complex (Nayarit and Jalisco, Mexico) recorded by the RESJAL network. IAVCEI General Assembly, Puerto Vallarta, Mexico, p. 129 1997 Abstracts.
Nelson, S.A., 1980. Geology and petrology of Volcán Ceboruco, Nayarit, Mexico. Geol. Soc. Am. Bull. 91, 2290–2431.
Nelson, S.A., 1986. Geología del Volcán Ceboruco, con una estimación de riesgos de erupciones futuras. Rev. Mex. Ciencias Geol., UNAM 6, 243–258.
Neuberg, J., 2000. External modulation of volcanic activity. Geophys. J. Int. 142, 232–240.
Nieto-Obregón, J., Delgado-Argote, L.A., Damon, P.E., 1985. Geochronologic, petrologic and structural data related to large morphological features between the Sierra Madre Occidental and the Mexican Volcanic Belt. Geofis. Int. 24, 623–663.
Núñez-Cornú, F.J., Rutz, M., Nava, F.A., Reyes-Dávila, G., Suárez-Plascencia, C., 2002. Characteristics of the seismicity in the coast and north of Jalisco, Block Mexico. Phys. Earth Planet. Inter. 132, 141–155.
Núñez-Cornú, F.J., Sánchez-Mora, C., 1999. Stress field estimations for Colima volcano, Mexico, based on seismic data. Bull. Volcanol. 60, 568–580.
Núñez-Cornú, F.J., Sandoval, J.M., Alarcón, E., Gómez, A., Suárez-Plascencia, D., Núñez, D., Trejo-Gómez, E., Sánchez-Mariscal, O., Candelas-Ortiz, J.G., Zúñiga-Medina, L.M., 2018. The Jalisco Seismic and Accelerometric Telemetric Network, (RESAJ). Seismo. Res. Lett. 89, 363–372. https://doi.org/10.1785/0220170157.
Núñez-Cornú, F.J., Escalona-Alcázar, F.J., Núñez, D., Trejo-Gómez, E., Suárez-Plascencia, C., Rodríguez-Ayala, N., 2020. Study of seismic activity at Ceboruco Volcano (Nayarit, Mexico) in the period 2012-2014. J. S. Am. Earth Sci. 98, 102473.
Petrone, C.M., 2010. Relationship between monogenetic magmatism and stratovolcanoes in western Mexico: the role of low-pressure magmatic processes. Lithos 119, 585–606.
Petrone, C., Francalanci, L., Ferrari, L., Schaaf, P., Conticelli, S., 2006. The San Pedro-Cerro Grande volcaninc complex (Nayarit, Mexico): inferences on volcanology and magma evolution. In: Siebe, C., Macías, J.L., Aguirre-Díaz, G. (Eds.), Neogene-Quaternary Continental Margin Volcanism: A Perspective from Mexico. Geological Society of America, Special Papervol. 402, pp. 65–98.
Petrosino, S., Cusano, P., Madonia, P., 2018. Tidal and hydrological periodicities of seismicity reveal new risk scenarios at Campi Flegrei caldera. Sci. Rep. 8, 13808.
Rodríguez-Castañeda, J.L., Rodríguez-Torres, R., 1992. Geología estructural y estratigrafía del área entre Guadalajara y Tepic, estados de Jalisco y Nayarit, México. 10. Universidad Nacional Autónoma de México, Instituto de Geología, Revista, pp. 99–110.
Rodríguez-Uribe, M.C., Núñez-Cornú, F.J., Nava Pichardo, F.A., Suárez-Plascencia, C., 2013. Some insights about the activity of the Ceboruco Volcano (Nayarit, Mexico) from recent seismic low-frequency activity. Bull. Volcanol. 75, 755.
Rydelek, P.A., Davis, P.M., Koyanagi, R.Y., 1988. Tidal triggering of earthquake swarms at Kilauea volcano, Hawaii. J. Geophys. Res. 93, 4401–4411.
Sánchez, J.J., Núñez-Cornú, F.J., Suárez-Plascencia, C., Trejo-Gómez, E., 2009. Seismicity at Ceboruco Volcano, México. Seismo. Res. Lett. 80, 823–830.
Sieron, K., 2009. Historia eruptiva, volúmenes emitidos y composición geoquímica e isotópica (sistemas Nd, Sr y Pb) del Volcán Ceboruco y edificios monogenéticos contiguos, estado de Nayarit, México. Doctoral disertation. UNAM, Mexico 152 pp (In Spanish).
Sieron, K., Siebe, C., 2008. Revised stratigraphy and eruption rates of Ceboruco Volcano and surrounding monogenetic vents (Nayarit, Mexico) from historical documents and new radiocarbon dates. J. Volcanol. Geoth. Res. 176, 241–264.
Sieron, K., Ferres, D., Siebe, C., Capra, L., Constantinescu, R., Agustín-Flores, J., González-Zuccolotto, K., Böhnel, H., Connor, L., Connor, C.B., Groppelli, G., 2019. Ceboruco Hazard Map: Part I – Definition of hazard scenarios based on the eruptive history. J. Appl. Volcanol. 8, 9.
Suárez-Plascencia, C., 1998. Análisis de las variables del riesgo volcánico en el Volcán Ceboruco, Nayarit, México. Master's thesisCentro de Investigación Científica y de Educación Superior de Ensenada 149 pp. (In Spanish).
Udías, A., Buforn, E., 1980. Earthquake mechanism and regional earthquake studies: Application to near earthquakes. Bollettino di Geofisica Teorica ed Applicatta, XXII 88, 321–327.
Wessel, P., Luis, J.F., Uieda, L., Scharroo, R., Wobbe, F., Smith, W.H.F., Tian, D., 2019. The generic mapping tools version 6. Geochem. Geophy. Geosy. 20, 5556–5564. https://doi.org/10.1029/2019GC008515.
White, R., McCausland, W., 2016. Volcano-tectonic earthquakes: a new tool estimating intrusive volumes and forecasting eruptions. J. Volcanol. Geoth. Res. 309, 139–155.
White, R., McCausland, W., 2019. A process-based model of pre-eruption seismicity patterns and its use for eruption forecasting at dormant stratovolcanoes. J. Volcanol. Geoth. Res. 382, 267–297.